Photonic Crystal Enhanced SERS Detection of Analytes Separated by Ultrathin Layer Chromatography Using a Diatom Frustule Monolayer

Joseph A. Kraai, Alan X. Wang, and Gregory L. Rorrer*

Diatoms are single-celled algae that biologically fabricate nanostructured silica shells with ordered pore arrays called frustules that resemble a 2D photonic crystal. A monolayer of *Pinnularia* frustules isolated from cell culture is deposited on a glass substrate and then conformally coated with silver nanoparticles (AgNPs) to serve as a nanostructured thin film for ultrathin layer chromatography (UTLC). Malachite green and Nile red are resolved in toluene mobile phase and the separated analytes are profiled micro-Raman spectroscopy, where plasmonic AgNPs provide surface-enhanced Raman scattering (SERS). The AgNP-diatom frustule monolayer improves SERS detection of malachite green by an average factor of 1.8 ± 0.1 over the plasmonic AgNP layer on glass. Analysis of hot spots on the AgNP-diatom frustule monolayer reveals that nearly 20% of the SERS active area intensifies the SERS signal at least tenfold over the SERS signal for AgNP on glass. Diatom-SERS enhancement is attributed to guided-mode resonances of the Raman laser source, which in turn further enhances the localized surface plasmonic resonance from AgNPs. Overall, the AgNP-diatom frustule monolayer thin film is a new functional material that uniquely enables separation of analytes by UTLC, quantitative SERS detection of separated analytes, and photonic enhancement of the SERS signals.

1. Introduction

Diatoms are single-celled algae that take up dissolved silicate in the form of $Si(OH)_4$, biomineralize intracellular $Si(OH)_4$ to SiO_2, and then fabricate nanostructured silica shells called frustules through a biologically mediated self-assembly process. Although the overall diatom cell size is typically several micrometers, the diatom frustule surface consists of ordered pore arrays hierarchically patterned at both the submicrometer and nanoscales.[1] Furthermore, diatom biosilica isolated from

J. A. Kraai, Prof. G. L. Rorrer
School of Chemical, Biological, and Environmental Engineering
Oregon State University
Corvallis, OR 97331, USA
E-mail: gregory.rorrer@oregonstate.edu
Prof. A. X. Wang
School of Electrical Engineering and Computer Science
Oregon State University
Corvallis, OR 97331, USA

The ORCID identification number(s) for the author(s) of this article can be found under https://doi.org/10.1002/admi.202000191.

cell culture is rich in silanol groups that can be readily functionalized.[2,3] Given these properties, diatom frustule biosilica is a versatile material for the fabrication of nanostructured devices, particularly for optoelectronic[4] and drug delivery applications.[5,6]

The ordered pore arrays of diatom frustule biosilica resemble a 2D photonic crystal and possess photonic properties[7] that enable their future use as optical waveguides, optical transducers,[8] and ultraviolet filters.[9] The addition of optically active materials to the diatom frustule imparts optoelectronic properties to the diatom photonic crystal. For example, the pennate diatom *Pinnularia* possesses a rectangular array of 200 nm diameter pores on 300 nm pitch. Excitation of *Pinnularia* diatom biosilica doped with GeO-rich nanophases selectively enhances electroluminescent emission wavelengths through resonant waveguide interactions within this porous structure.[10] Similarly, in vivo incorporation of organic fluorophores into the diatom biosilica matrix significantly enhances fluorescent light emission.[11]

The integration of metal plasmonic and dielectric photonic crystal structures holds significant promise for improving the sensitivity of surface-enhanced Raman scattering (SERS) for chemical analysis.[12,13] In particular, when the diatom frustule surface is decorated with silver nanoparticles (AgNPs), localized surface plasmon resonance (LSPR) generated by visible laser excitation of the AgNPs greatly intensifies the Raman scattering signal of solute molecules adsorbed onto the diatom frustule biosilica. The submicrometer pore arrays on the diatom frustule further enhance the LSPR through guided-mode resonances at visible wavelengths. This in turn leads to a marked increase the SERS signals, particularly at hot spots where AgNPs reside at the pore rim or within the pore, as demonstrated in previous experimental and computational studies.[14–20] Electroless deposition of gold onto the diatom frustule surface also enhanced Raman scattering signal intensity, which was attributed to the diatom nanoscale features.[21]

SERS detection of multicomponent mixtures is also facilitated by chromatographic separation of the analytes in the mixture. In particular, SERS has been used to identify and enhance detection of analytes separated by thin layer chromatography (TLC) using TLC plates coated with silver or gold nanoparticles. In most of these systems, the stationary phase material was porous silica
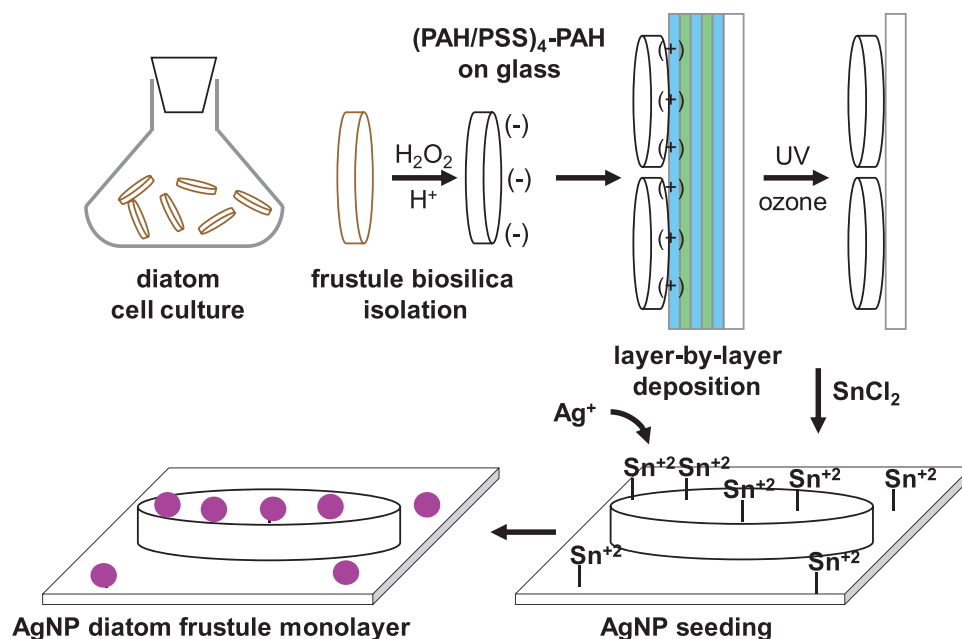
Figure 1. Fabrication of the AgNP-diatom frustule biosilica monolayer on glass (not to scale).

gel. To enable SERS detection, metal nanoparticles were sprayed onto the TLC substrate after the chromatographic separation[22–27] or infiltrated into the film.[28,29] Metal nanostructures were also incorporated onto silicon nanowires by top-down fabrication techniques to serve as SERS-TLC devices.[30,31]

Previously, we demonstrated that the use of diatom frustule biosilica as a stationary phase for conventional TLC improved separation performance relative to silica gel, due to enhanced mass transfer of the analytes through the highly porous matrix of diatom frustule.[3] Furthermore, we recently developed a process to conformally grow silver nanoparticles onto the porous surface of the diatom frustule by reduction of silver nitrate ($AgNO_3$) onto biosilica seeded with Sn^{+2}.[20]

Ultrathin layer chromatography (UTLC) is defined by a stationary phase layer thickness of less than 10 μm and solvent migration distance of less than 3 cm to provide a high separation efficiency and sensitivity relative to conventional TLC.[32] In this study, we describe the bottom-up fabrication of a nanostructured thin film composed of a diatom biosilica frustule monolayer decorated with AgNPs for SERS-UTLC. A polyelectrolyte layer-by-layer (LbL) technique is used to deposit a single layer of diatom frustules on a glass surface and AgNPs are conformally grown onto the pore arrays of the frustule surface. This new functional material enables separation of analytes by UTLC, SERS detection of separated analytes, *and* photonic enhancement of the SERS signals, as reported below.

2. Results and Discussion

2.1. Fabrication of AgNP-Diatom Biosilica Frustule Monolayer Thin Films

The fabrication of the AgNP-diatom biosilica frustule monolayer on glass is overviewed in **Figure 1**. Biosilica frustules of the pennate diatom *Pinnularia* sp. were isolated from cultured cells by treatment with aqueous hydrogen peroxide (H_2O_2) and then deposited as monolayer on glass using a polyelectrolyte layer-by-layer dip-coating technique. By this technique, four bilayers of positively charged poly(allyamine hydrochloride) (PAH) and negatively charged poly(sodium 4-styrene sulfonate) (PSS) were coated onto a glass surface. A fifth (top) layer of PAH promoted adhesion of the negatively charged frustule biosilica to this surface.[33]

Scanning electron microscopy (SEM) images of isolated diatom frustules before deposition on a glass surface are presented in **Figure 2**a,b. Isolated *Pinnularia* frustules were ellipsoidal in shape (Figure 2a). The average frustule dimensions are presented in **Table 1**. The diatom frustule surface consisted of rectangular pore arrays with nominal diameter of 200 nm and center-to-center pitch of nominally 300 nm. Lining the base of each 200 nm pore was a thin layer of biosilica containing four to five pores of nominally 50 nm (Figure 2b). A given diatom cell possessed two frustules, an upper half and a lower half (thecae), that separated during the frustule isolation process. Each frustule theca contained a valve (top face) and a girdle band lining the valve rim and the frustule thickness was nominally 100 nm.

SEM images of *Pinnularia* diatom frustule monolayers on glass decorated with AgNPs are presented in Figure 2c–f. Diatom frustule monolayer thin films were prepared on glass slides cut to 2.5 mm width and 15 mm length. Generally, a monolayer of biosilica frustules adhered to the (PAH-PSS)$_4$-PAH coated glass surface, although some stacking of frustules occurred due to incomplete contact of the valve face on the surface (Figure 2c,d). Furthermore, although of most the frustules adhered to the surface valve face down, some were adhered to the surface at the girdle band. The typical height of the frustule adhered to the surface was generally under 5 μm. The average number of frustules deposited on the surface was 2600 ± 400 frustules mm^{-2}
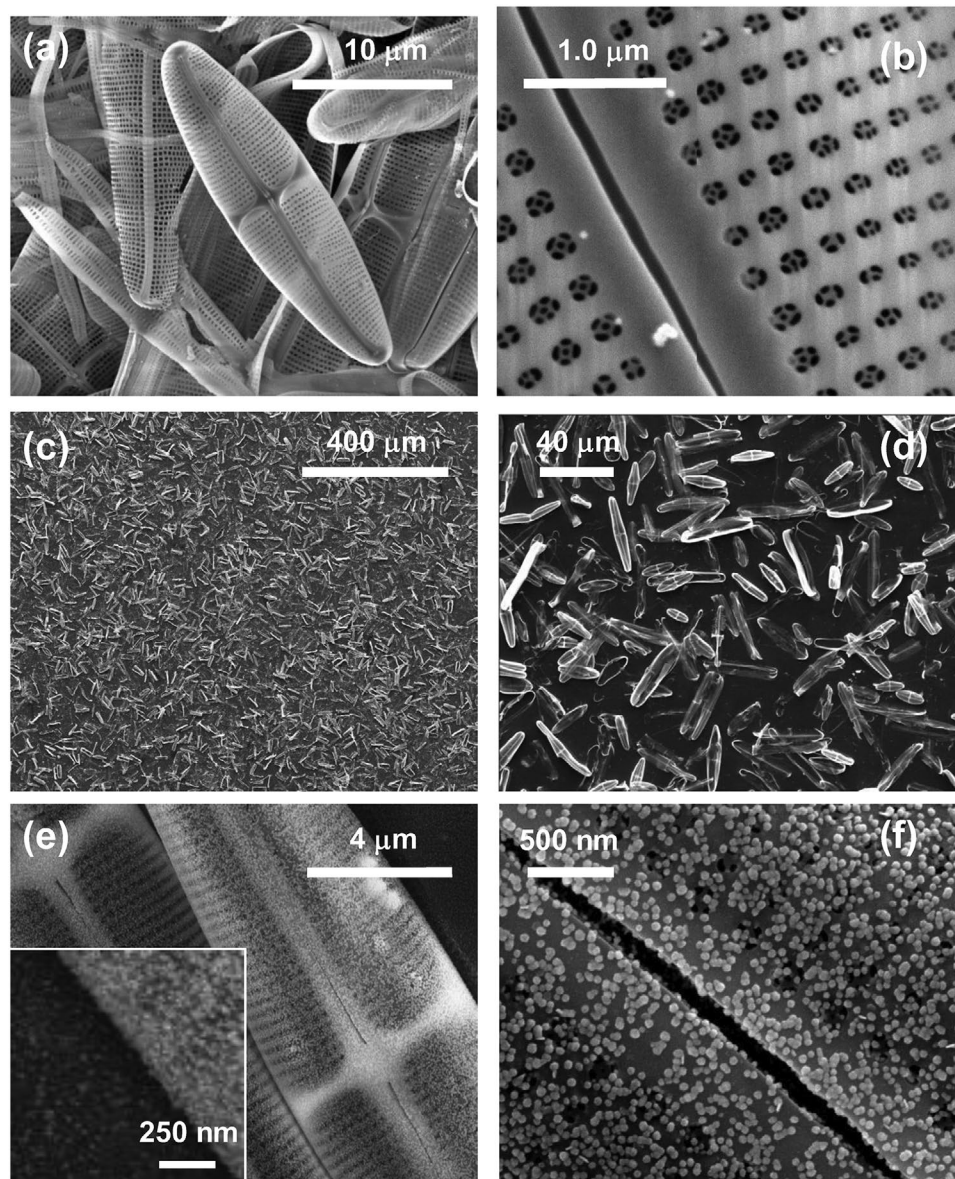
**ADVANCED
SCIENCE NEWS**

www.advancedsciencenews.com

**MATERIALS
INTERFACES**

www.advmatinterfaces.de

Figure 2. SEM images of frustules from the pennate diatom *Pinnularia* sp. a,b) Isolated frustules before deposition onto PAH-coated glass. c,d) AgNP-diatom frustule monolayer on glass. e,f) Close-up of AgNP-diatom frustule surface showing conformal coating of AgNPs.

(1.0 standard deviation (S.D.), *n* = 3 thin film preparations). Based on the known biosilica content of *Pinnularia* diatom cells of 7.2×10^8 cells mmol^{-1} Si,[1] the estimated loading of diatom frustules on the thin film was $\approx$10 µg SiO$_2$ cm^{-2}.

An in situ Ag+ nucleation process described previously[20] deposited silver nanoparticles of 43 nm average diameter on the diatom biosilica and surrounding glass substrate. The AgNPs were conformally deposited as a dispersed single layer on the diatom frustule outer surface and were generally separated from one another, although there were some regions of close packing. AgNPs were also deposited within the 200 nm pores (Figure 2e,f). SEM-energy dispersive X-ray (EDX) analysis of four randomly selected AgNP diatom frustules determined that total amount of silver deposited on the diatom biosilica was 16.6 ± 1.5 g Ag/100 g SiO$_2$ (1.0 S.D., *n* = 4). The size and surface coverage of AgNPs

seeded and grown on the surrounding glass layer were consistent with those on the diatom frustule (inset Figure 2e).

The UV–vis absorbance spectrum of the diatom biosilica frustule monolayer on glass before and after conformal coating with AgNPs is compared in **Figure 3**. Also provided is the UV–vis absorbance spectrum from the AgNP layer on glass, not colloidal AgNPs. The absorbance increased for the AgNP-diatom frustule biosilica monolayer versus AgNP on the glass surface alone. The appearance of the peak at 424 nm most likely comes from the blueshift of the broad 459 nm peak of AgNPs on glass because the AgNP layer on glass would have higher surrounding refractive index than AgNPs coated on the thin, porous diatom biosilica frustule monolayer.

Assessments of surface wetting characteristics and long-term stability of the AgNP-diatom biosilica frustule monolayer thin

ADVANCED
SCIENCE NEWS
www.advancedsciencenews.com

MATERIALS
INTERFACES
www.advmatinterfaces.de

Table 1. Structure and mobile phase flow properties of AgNP-diatom biosilica frustule monolayer thin film on glass.

Property	Value
Major axis frustule length [µm]	19 ± 6 (1.0 S.D., $n = 158$)
Minor axis frustule width [µm]	8 ± 3 (1.0 S.D., $n = 158$)
Frustule loading on surface [particles mm^{-2}]	2600 ± 400 (1.0 S.D., $n = 3$)
AgNP on biosilica [g Ag/100 g SiO$_2$]	16.6 ± 1.5 (1.0 S.D., $n = 4$)
AgNP diameter [nm]	43 ± 18 (1.0 S.D., $n = 5679$)
Mobile phase velocity constant, χ [cm^2 s^{-1}]	$1.3 \times 10^{-2} \pm 9 \times 10^{-4}$ (1.0 S.E.)
Mobile phase permeability, k_o [dimensionless]	$1.1 \times 10^{-3} \pm 8 \times 10^{-5}$ (1.0 S.E.)

films, which would be necessary for UTLC device performance optimization, were not performed in this study.

2.2. AgNP-Diatom UTLC with SERS Detection

In all diatom-SERS UTLC analyses, the mobile phase solvent (toluene) was allowed to advance 12.0 mm with an average elution time of 180 s. Solvent front versus time data were analyzed by the Lucas–Washburn equation for capillary flow as described previously.[3] Least-squares estimates for solvent flow velocity (χ) and flow permeability (k_o) constants for wicking solvent flow through the AgNP-diatom frustule biosilica monolayer are presented in Table 1.

Nile red and malachite green were chosen as the model analytes to demonstrate the separation performance of the diatom-SERS UTLC thin film. Nile red is nonpolar phenoxazine dye ($C_{20}H_{18}N_2O_2$, mol. wt. 318.37 g mol^{-1}), whereas malachite green is a weakly cationic triphenylmethane dye with two *N*-dimethyl groups ($C_{23}H_{25}N_2Cl$, mol. wt. 364.91 g mol^{-1}). Therefore, Nile red is expected to be more mobile than malachite green in the nonpolar toluene elution solvent. The elution of Nile red

Figure 3. Absorbance spectra of AgNP-diatom frustule monolayer on glass, AgNP layer on glass, and diatom frustule monolayer on glass.

and malachite green on the AgNP-diatom frustule monolayer thin film was profiled by micro-Raman spectroscopy (400–1800 cm^{-1}) at 0.9 µm spot width and increments of 0.1 mm along the length of the UTLC plate (**Figure 4**a). The chromatographically resolved analytes were dispersed across the 2.5 mm width of the UTLC plate (Figure S1, Supporting Information). The UTLC analyses were carried out at initial loadings of 1.58–158 ng for each analyte and so the apparent sample loadings analyzed within the cross-section of the Raman laser line (0.9 µm thickness) ranged from 0.57 to 57 pg.

Figure 4b shows the full Raman spectrum at 1.0 mm measurement intervals along the UTLC plate. **Figure 5**a provides a more detailed line scan of Raman signal measurements at 0.1 mm intervals for Raman wavenumbers 590 and 1615 cm^{-1}, which are signature signals for Nile red and malachite green, respectively. Figure 5b shows the profile around the 9.0 mm peak at 590 cm^{-1} for two separately prepared AgNP-coated diatom frustule monolayer thin films. Malachite green and Nile red were fully resolved from one another. However, comparison of the full Raman spectrum of the resolved peaks showed that some of Nile red was still associated with the malachite green peak (Figure 5c), whereas the Nile red peak was essentially pure (Figure 5d).

The Raman signal versus position profile was not smooth and possessed spikes and valleys. The position of the peaks and valleys appeared random and did not line up for two separate UTLC film preparations. The repeatability of the chromatogram was also affected by the discrete Raman signal sampling distance of 0.1 mm. However, the integrated peak areas were consistent between UTLC film preparations. Peak area (A_s) versus amount of analyte in the micro-Raman scanning cross-section (m_s) for malachite green (1615 cm^{-1}) and Nile red (590 cm^{-1}) are presented in **Figure 6**. Figure 6 demonstrates that sensitivity of Nile red was about two times higher than malachite green over a two-order of magnitude change in concentration. Furthermore, both compounds were detectable to 0.6 pg in the line scan (1.6 ng in the total spot). No attempt was made to identify or optimize the limits of detection because this value would also be dependent on micro-Raman signal acquisition time and analysis spot size, which were not varied. Control experiments verified that after the AgNPs were added to the diatom biosilica, the average Raman signal intensity at 1615 cm^{-1} for malachite green increased by a factor of 118, demonstrating the strong effect of the LSPR on Raman scattering (Figure S2, Supporting Information).

2.3. Photonic Enhancement of SERS by the Diatom Frustule Monolayer

It was noted above that the SERS signal versus position profile on the diatom SERS-UTLC thin film was not smooth and was punctuated by spikes and valleys as the analyte was being chromatographically resolved. This phenomenon was observed for all experiments and so appeared to be an intrinsic feature of the system, not measurement error. The plume for each separated analyte spot was observed to be uniformly distributed on the thin film. However, it appeared that when the micro-Raman laser hit the AgNP-diatom frustule itself versus
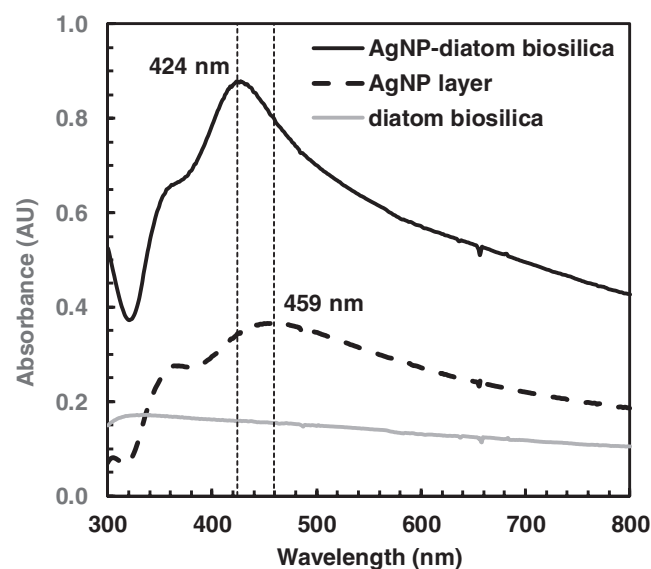
**ADVANCED
SCIENCE NEWS**
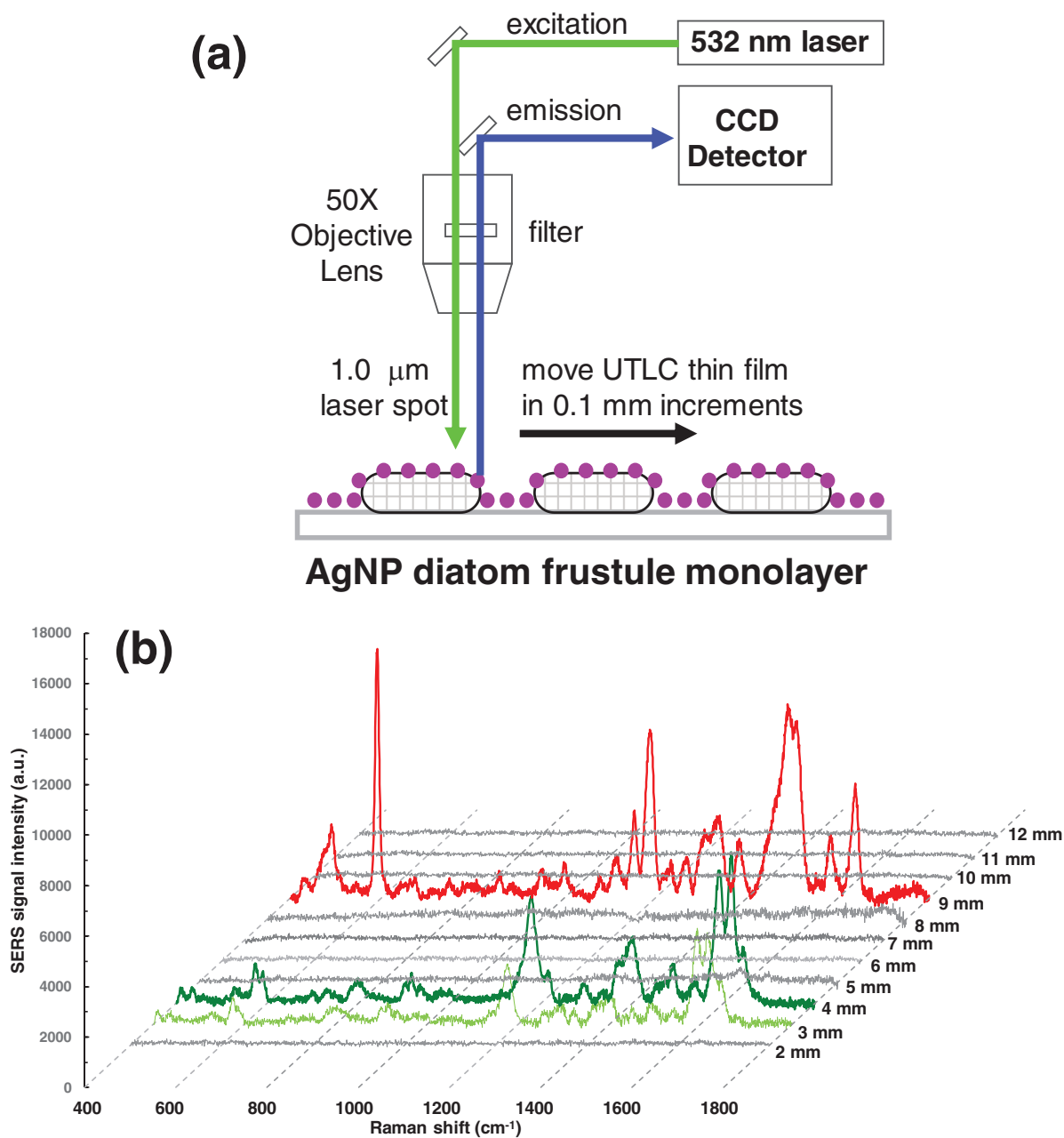www.advancedsciencenews.com

**MATERIALS
INTERFACES**
www.advmatinterfaces.de

Figure 4. Diatom-SERS UTLC. a) Process for micro-Raman line scan of diatom-SERS UTLC thin film (not to scale). b) Raman spectrum (400–1800 cm^{-1}) versus position on the diatom-SERS UTLC thin film after chromatographic separation of malachite green and Nile red (toluene solvent front ended at 12 mm).

the surrounding AgNP layer, the strength of the Raman signal increased. To investigate this phenomenon in more detail, micro-Raman maps at 3.0 µm resolution were obtained in a 36 µm by 42 µm box around a single AgNP diatom frustule and surrounding AgNP layer on glass associated with the malachite green spot. Within this box, malachite green was present on both the AgNP-diatom frustule and the surrounding AgNP layer on glass. A representative microscopic image and its complimentary Raman heat map at the characteristic 1615 cm^{-1} Raman signal for malachite green are presented in **Figure 7**a,b, respectively. The light microscope

image clearly showed the boundary between the AgNP-diatom frustule and the surrounding AgNP layer on glass. Hot spots were clearly evident on the AgNP-diatom frustule but less so on the surrounding AgNP layer on glass.

By choosing the lowest SERS signal intensity (I_{ref}) in the analysis area as the reference point, the normalized distribution of SERS signal intensities at 1615 cm^{-1} for both the AgNP-diatom frustule monolayer ($I' = I/I_{ref}$) and the surrounding AgNP layer on glass ($I'_o = I_o/I_{ref}$) were compared, as shown in Figure 7c. In Figure 7d, data were pooled from nine randomly selected frustules from two separate UTLC thin film preparations. The ratio
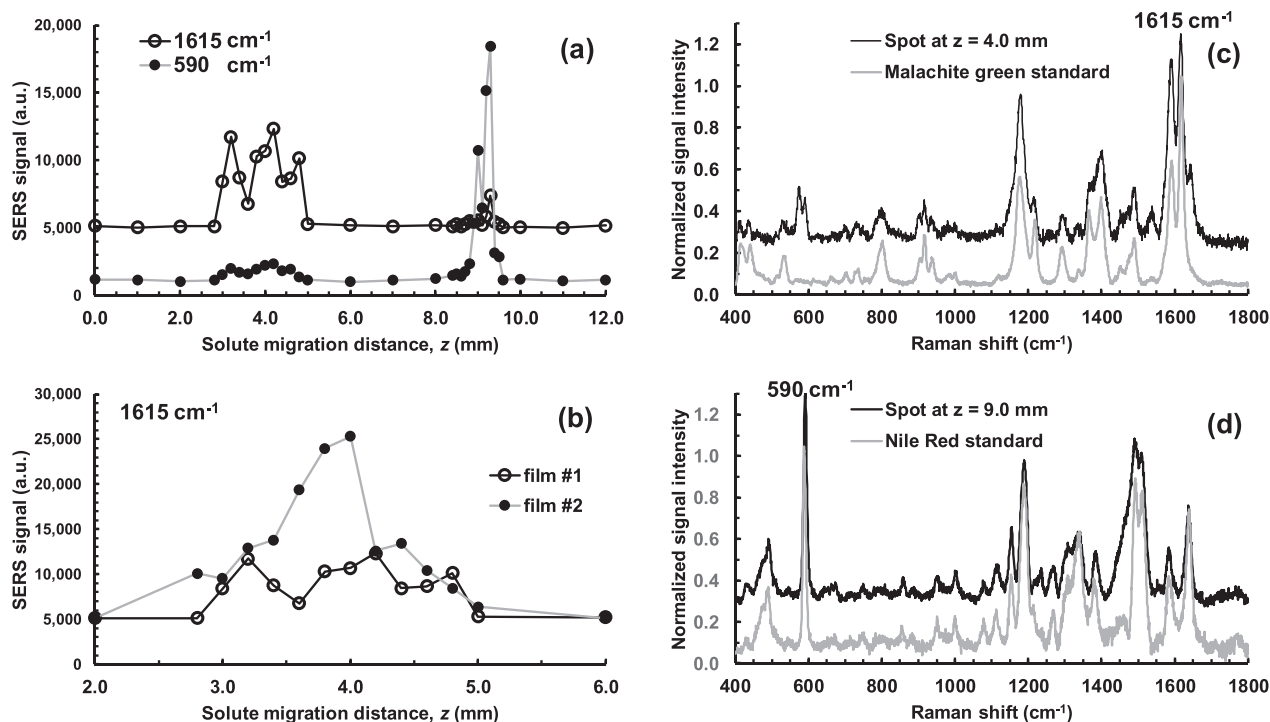
Figure 5. SERS-UTLC chromatogram for separation of malachite green and Nile red on AgNP-diatom frustule monolayer thin film. a) Line scans at 590 and 1615 cm^{-1}. b) Comparison of Nile red peak at 590 cm^{-1} from two separately prepared films. c) SERS spectra of UTLC-eluted spot for malachite green ($z = 4.0$ mm). d) SERS spectra of UTLC-eluted spot for and Nile red ($z = 9.0$ mm).

of I' (AgNP-diatom frustule monolayer) and I'_o (AgNP on glass), given by $EF_{DS} = I'/I'_o$, was consistently between 1.5 and 2.0. The average enhancement factor for SERS detection of the analyte on the AgNP-diatom frustule monolayer relative to the AgNP layer on glass (average of all EF_{DS} values) was defined as

$$EF_{DS,av} = \frac{\frac{1}{n}\sum_1^n I'}{\frac{1}{m}\sum_1^m I'_o} \tag{1}$$

with $EF_{DS,av} = 1.8 \pm 0.1$ (1.0 standard error (S.E.)). The frequency distribution of EF_{DS} values revealed a relatively broad SERS

signal enhancement range for AgNP-diatom frustule versus AgNP on glass, with 19% of sites exhibiting hot spot behavior with signals at or exceeding ten times the reference signal within the SERS active area.

Figure 8 summarizes the processes associated with the photonic enhancement of the SERS signals. When the excitation light source (532 nm Raman laser) is coupled to the guided mode resonances within the diatom frustule pore array, the electromagnetic field intensity generated by LSPR of the AgNPs on the diatom frustule becomes enhanced relative to the intensity of the excitation. Consequently, there is a commensurate local enhancement of the SERS signals associated with the analyte molecule on the diatom frustule biosilica. Together, these processes create the photonic crystal enhancement leading to
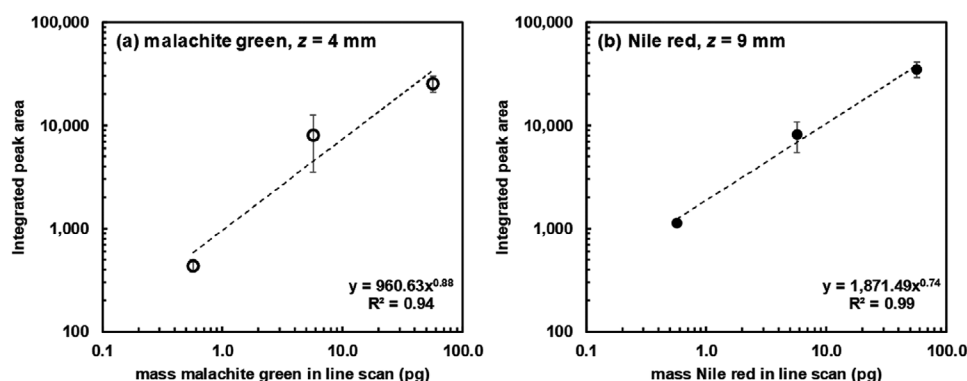

Figure 6. Integrated peak areas from SERS line scan. a) Malachite green at 1615 cm^{-1}. b) Nile red at 590 cm^{-1}.

ADVANCED
SCIENCE NEWS
www.advancedsciencenews.com

MATERIALS
INTERFACES
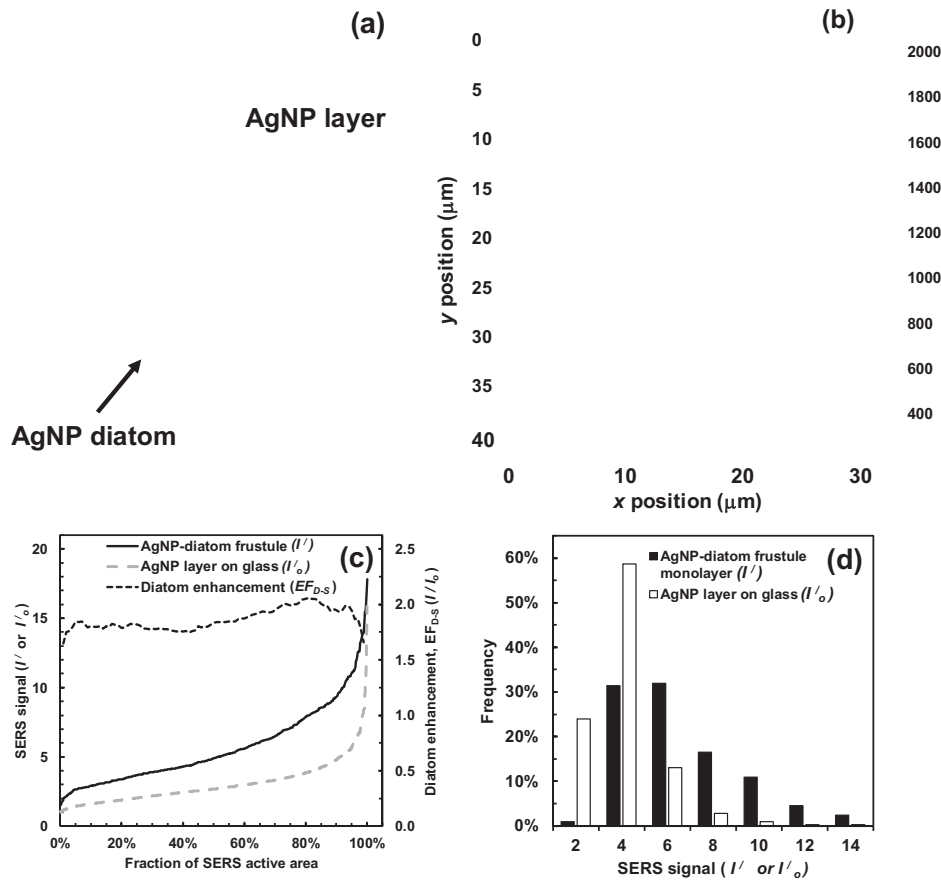www.advmatinterfaces.de

Figure 7. Distribution of Raman signals from eluted analytes on the AgNP-diatom frustule versus surrounding AgNP on glass for malachite green analyte spot. a) Light microscope image of single representative AgNP-diatom frustule and surrounding AgNP layer. b) Raman signal heat map at 1615 cm⁻¹ for same light microscope image. c,d) Cumulative and frequency distributions of SERS signal intensities at 1615 cm⁻¹ for malachite green on the AgNP-coated diatom frustule versus the surrounding AgNP on glass, normalized to a baseline signal for nine randomly selected AgNP-diatom frustules.

the SERS hot spots on the AgNP-diatom frustule. These hot spots are likely associated with AgNPs residing at the pore rim or within the pore.[14,18,19] This enhancement is not attributed to the irreversible adsorption of the analytes onto the AgNP-diatom biosilica relative to AgNP on glass. Although malachite green weakly adsorbs onto silica in aqueous solution,[34] it was assumed that both malachite green and Nile red did not irreversibly partition into the stationary phase in a nonpolar toluene mobile phase.
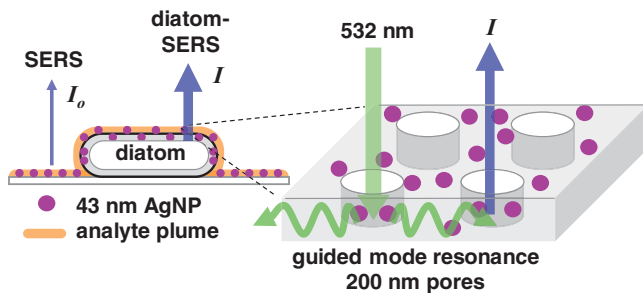

Figure 8. Schematic representation of SERS signal intensity of separated analyte plume around AgNP-diatom frustule monolayer versus AgNP on glass, illustrating the guided-mode resonance effect.

In the context of the above discussion, AgNP spacing could not be precisely arrayed on the diatom frustule surface, and so hot spots were likely generated from only a fraction of the deposited AgNPs. Future work would adjust the Ag⁺ seeding process to vary the number density of AgNPs deposited on the surface. From this information, the optimal AgNP loading for maximizing SERS signal response could be determined. Previous studies have shown how rational optimization of nanostructure enhances SERS.[35–39]

The diatom-SERS UTLC thin film offers quantitative analysis of the separated analytes by peak area integration of signature SERS signals from the laser line scan, combined with enhanced limits of detection if 2D mapping is used to harvest SERS signals from local hot spots. The small footprint of the diatom-SERS UTLC thin film device suggests that it could be integrated into future microfluidic systems that require analyte separation and detection at small sample volume.

3. Conclusions

This study showed that AgNP-diatom frustule monolayer can serve as an SERS-UTLC thin film, where the SERS signal used

**ADVANCED
SCIENCE NEWS**

www.advancedsciencenews.com

**MATERIALS
INTERFACES**

www.advmatinterfaces.de

to detect and quantify the separated analytes was enhanced through the photonic properties of the diatom biosilica frustule pore array.

A monolayer of diatom biosilica frustules was deposited on a glass substrate through a polyelectrolyte layer-by-layer process. AgNPs were then conformally grown on the surface and within the pores of the frustule pore array. The AgNP-diatom frustule monolayer improved quantitative SERS detection of the separated analyte malachite green by an average factor of 1.8 ± 0.1 over the surrounding plasmonic AgNP layer on glass. Furthermore, distribution analysis of hot spots on the AgNP-diatom frustule monolayer revealed that nearly 20% of the SERS active area intensified the SERS signal at least tenfold over the SERS signal for AgNP on glass. This enhancement is attributed to the photonic properties of the AgNP-diatom frustule monolayer thin film. Specifically, the 200 nm pore arrays on the diatom frustule provided guided-mode resonances of the Raman laser excitation source within the visible wavelength range. This photonic process in turn enhanced the localized surface plasmonic resonance from AgNP decorating the ordered pore arrays on the frustule surface, resulting in an increase in the SERS signals associated with the chromatographically separated analyte, consistent with earlier studies where a pure analyte was deposited directly onto the AgNP-coated diatom biosilica.[14,18,19]

In summary, the AgNP-diatom frustule monolayer uniquely combines the functions of UTLC separation, SERS detection of separated analytes, *and* the photonic enhancement of these SERS signals into a single platform. Furthermore, this new functional material is fabricated through a combination of biological and chemical self-assembly processes at ambient temperature, where nanostructured diatom frustules are isolated from cultured cells and silver nanoparticles are seeded and grown on this nanostructured substrate. This approach offers a simple and flexible means for fabrication of multifunctional, nanostructured thin film materials with unique optical properties.

4. Experimental Section

Fabrication of Diatom Frustule Monolayers on Polyelectrolyte Multilayer (PEM)-Coated Glass Substrates: Photosynthetic cells of the pennate diatom *Pinnularia* sp. (UTEX B679) were cultured in artificial seawater medium, isolated by centrifugation, treated with aqueous HCl/H_2O_2 to remove organic materials by chemical oxidation and then collected by gravity settling as described previously to isolate intact biosilica frustules.[1,3]

Biosilica frustule monolayers were deposited onto washed, UV-ozone cleaned (90 °C, 24 h) glass surface possessing a net positive surface charge prepared by LbL PEM adsorption technique. The polyelectrolyte pair was positively charged poly(allylamine hydrochloride) (PAH) and negatively charged PSS. Glass substrates (2.5 mm by 15 mm, 1.0 mm thickness) were immersed in a 1.35 mg mL^{-1} solution of PAH in 0.5 M NaCl at pH 6 under continuous mixing for 1 min, rinsed 3X in nanopure water (10 s per rinse), dipped in 3.0 mg mL^{-1} PSS in 0.5 M NaCl at pH 6 under continuous mixing for 1 min, and then rinsed 3X in nanopure water (10 s per rinse). The PAH/PSS deposition step was repeated four times, ending with a fifth top layer of positively charged PAH, and then dried under flowing N_2 gas at 22 °C. Diatom biosilica frustules with a net negative charge[33] were gently dispersed in nanopure water at pH 7 to a concentration of 6.5 mg mL^{-1}. A 100 µL aliquot of this suspension

was evenly dispensed onto each positively charged (PAH/PSS)$_4$-PAH substrate. Each substrate was placed in an orbital shaker at 120 rpm for 20 min at 22 °C, rinsed 3X in nanopure water (15 s per rinse), dried under flowing N_2 gas at 22 °C, and then treated in a UV-ozone cleaner at 90 °C for 24 h to oxidize PEMs and residual organic contaminants on the frustule surface. The UV-ozone treatment also fixed the biosilica frustule monolayer to the underlying glass substrate. Diatom biosilica frustule monolayers were stored under vacuum desiccation until use.

In Situ Growth of Silver Nanoparticles on Diatom Frustule Biosilica Monolayers: An in situ AgNP growth method adapted from previous work[20] was used to uniformly deposit AgNPs onto the diatom frustule monolayer. Diatom frustule monolayer substrates were immersed 104 mL of 20×10^{-3} M SnCl$_2$/20×10^{-3} M HCl and continuously mixed on an orbital shaker at 160 rpm for 2 min at 22 °C to deposit Sn^{+2} nuclei on silanol (SiOH) sites of the frustule biosilica. In the silver (Ag) nucleation process, the Sn^{+2}-seeded diatom frustule monolayers were rinsed with nanopure water and acetone, dried under flowing N_2 gas, and then immersed in 10 mL of 20×10^{-3} M AgNO$_3$ under continuous mixing on an orbital shaker at 160 rpm for 30 min a 22 °C. At the seeding site, Ag^{+2} was reduced according to the reaction Sn^{+2} + 2 Ag$^+$ → Sn^{+4} + 2 Ag (adsorbed). Silver-seeded diatom frustule monolayers on glass were rinsed with H_2O and acetone and then dried under flowing N_2 gas. In the AgNP growth process, Ag-seeded diatom frustule monolayers were immersed in 104 mL of 2:1 v/v 5.0×10^{-3} M AgNO$_3$/20×10^{-3} M ascorbic acid reducing agent, continuously mixed on an orbital shaker at 160 rpm for 30 min, rinsed with water and acetone, dried under flowing N_2 gas, and then stored under vacuum desiccation until use.

Characterization of AgNP-Diatom Frustule Biosilica Monolayers: The UV–vis absorbance spectra of diatom frustule monolayers on glass, AgNP monolayers on glass, and AgNP-diatom frustule monolayers on glass were obtained by placing the substrates directly in the optical path of Shimadzu Multi-Spec 1501 photodiode array sprectrophotometer, subtracted for the background spectra of washed, UV-ozone cleaned glass. Diatom frustule monolayers before and after AgNP deposition were profiled by SEM/EDX analysis. Substrates were sputtered with gold (9 nm coating) before analysis. SEM/EDX data were acquired on an FEI Company Quanta 600 field emission gun-SEM with an accelerating voltage of 10.00–15.00 kV, with 6 µm^2 analysis area for EDX elemental analysis. Diameter of AgNPs was estimated from analysis of 5 SEM images (50 000x) on ImageJ software.

Ultrathin-Layer Chromatography (UTLC): The AgNP-diatom frustule monolayer on glass (2.5 mm width and 15 mm length) served as the plate for UTLC. Reference analytes selected to assess UTLC separation were the triphenylmethane dye malachite green ($C_{23}H_{25}N_2Cl$, mol. wt. 364.91 g mol^{-1}, chemical abstracts service (CAS) Number 569-64-2) and the phenoxazine dye Nile red ($C_{20}H_{18}N_2O_2$, mol. wt. 318.37 g mol^{-1}, CAS Number 7385-67-3). The mobile phase (elution solvent) used for all UTLC experiments was high purity (99.9%) toluene. At 22 °C, liquid toluene has a density of 0.865 g cm^{-3}, viscosity of 0.58 cP, and surface tension of 28.266 dyne cm^{-1}. A UTLC developing chamber similar to previous work[3] was used to carry out the chromatographic separation process. A 200 nL aliquot of analyte solution containing Nile red and malachite green in ethanol (1:1 malachite green to Nile red by mass) was dispensed onto an AgNP-diatom frustule monolayer at a sample origin of 4 mm from the edge of the plate as a 2.0 ± 0.2 mm (1.0 S.D., $n = 3$) spot. The concentration of Nile red or malachite green in the analyte solution ranged from 10 to 1000 µg analyte g^{-1} solvent, which corresponded to 1.57–157 ng of each analyte loaded onto the diatom SERS-UTLC thin film. Capillary action at the interface between the AgNP-diatom frustule monolayer (stationary phase) and toluene solvent (mobile phase) drove wicking flow of the mobile phase flow up through the stationary phase. When the mobile phase front reached a final migration distance of 12 mm, UTLC development was stopped by removing the stationary phase from the development chamber. After toluene had visibly evaporated from the stationary phase, the developed UTLC plate was placed on a hot plate surface at 45 °C for 10 s to ensure complete mobile phase evaporation and then immediately profiled by micro-Raman spectroscopy.

**ADVANCED
SCIENCE NEWS**

www.advancedsciencenews.com

**MATERIALS
INTERFACES**

www.advmatinterfaces.de

Micro-Raman Spectroscopy of Diatom SERS-UTLC: A Horiba Jobin Yvon LabRAM HR800 Raman microscope acquired full Raman spectra at 0.1–0.2 mm increments over the 12 mm length of the developed diatom SERS-UTLC plate, using a mechanical stage caliper and on-stage micrometer. Spectra were acquired from 400 to 1800 cm^{-1} using a 532 nm laser excitation wavelength, 3 s acquisition time, one accumulation, 200 μm confocal hole diameter, and 50x objective magnification with a laser beam diameter of 0.9 μm. Within the 0.9 μm analysis cross-section, 0.57–57 pg of each analyte was profiled versus 1.58–158 ng loaded onto the 2.5 mm width of the UTLC plate. Nine Raman maps were acquired around randomly selected AgNP-coated diatom frustules. The typical dimensions of areas analyzed via Raman mapping were 36 μm by 42 μm with spectra acquired in 3 μm increments. Raman maps were acquired from 400 to 800 cm^{-1} across this area with a laser excitation wavelength of 532 nm, 0.5 s acquisition time, one accumulation, 200 μm confocal hole diameter, 50x objective magnification, laser spot size of 0.9 μm, and filter power set to 10%.

Supporting Information

Supporting Information is available from the Wiley Online Library or from the author.

Conflict of Interest

The authors declare no conflict of interest.

[1] C. Jeffryes, T. Gutu, J. Jiao, G. L. Rorrer, *Mater. Sci. Eng., C* **2008**, *28*, 107.

[2] D. K. Gale, T. Gutu, J. Jiao, C.-H. Chang, G. L. Rorrer, *Adv. Funct. Mater.* **2009**, *19*, 926.

[3] J. A. Kraai, G. L. Rorrer, A. X. Wang, *J. Chromatogr. A* **2019**, *1591*, 162.

[4] G. L. Rorrer, in *Diatom Nanotechnology: Progress and Emerging Applications* (Ed: D. Losic), Royal Society of Chemistry, London, UK **2018**, pp. 79–110.

[5] I. Rea, M. Terracciano, L. De Stefano, *Adv. Healthcare Mater.* **2017**, *6*, 1601125.

[6] M. Terracciano, L. De Stefano, I. Rea, *Pharmaceutics* **2018**, *10*, 242.

[7] E. De Tommasi, *J. Spectrosc.* **2016**, *2016*, 13.

[8] L. De Stefano, P. Maddalena, L. Moretti, I. Rea, I. Rendina, E. De Tommasi, V. Mocella, M. De Stefano, *Superlattices Microstruct.* **2009**, *46*, 84.

[9] Y. Su, T. A. Lenau, E. Gundersen, J. J. K. Kirkensgaard, C. Maibohm, J. Pinti, M. Ellegaard, *Sci. Rep.* **2018**, *8*, 959.

[10] C. Jeffryes, R. Solanki, Y. Rangineni, W. Wang, C. Chang, G. L. Rorrer, *Adv. Mater.* **2008**, *20*, 2633.

[11] R. Ragni, F. Scotognella, D. Vona, L. Moretti, E. Altamura, G. Ceccone, D. Mehn, S. R. Cicco, F. Palumbo, G. Lanzani, G. M. Farinola, *Adv. Funct. Mater.* **2018**, *28*, 1706214.

[12] B. Liu, H. Monshat, Z. Gu, M. Lu, X. Zhao, *Analyst* **2018**, *143*, 2448.

[13] A. X. Wang, X. Kong, *Materials* **2015**, *8*, 3024.

[14] F. Ren, J. Campbell, X. Wang, G. L. Rorrer, A. X. Wang, *Opt. Express* **2013**, *21*, 15308.

[15] J. Yang, L. Zhen, F. Ren, J. Campbell, G. L. Rorrer, A. X. Wang, *J. Biophotonics* **2015**, *8*, 659.

[16] N. Chamuah, L. Chetia, N. Zahan, S. Dutta, G. A. Ahmed, P. Nath, *J. Phys. D: Appl. Phys.* **2017**, *50*, 175103.

[17] X. Kong, Y. Xi, P. Le Duff, X. Chong, E. Li, F. Ren, G. L. Rorrer, A. X. Wang, *Biosens. Bioelectron.* **2017**, *88*, 63.

[18] X. Kong, K. Squire, E. Li, P. Leduff, G. L. Rorrer, S. Tang, B. Chen, C. P. Mckay, R. Navarro-Gonzalez, A. X. Wang, *IEEE Trans. NanoBiosci.* **2016**, *15*, 828.

[19] X. Kong, Y. Xi, P. Leduff, E. Li, Y. Liu, L. J. Cheng, G. L. Rorrer, H. Tan, A. X. Wang, *Nanoscale* **2016**, *8*, 17285.

[20] K. Sivashanmugan, K. Squire, J. A. Kraai, A. Tan, Y. Zhao, G. L. Rorrer, A. X. Wang, *Adv. Opt. Mater.* **2019**, *7*, 1900415.

[21] M. Pannico, I. Rea, S. Chandrasekaran, P. Musto, N. H. Voelcker, L. De Stefano, *Nanoscale Res. Lett.* **2016**, *11*, 315.

[22] D. Li, L. Qu, W. Zhai, J. Xue, J. S. Fossey, Y. Long, *Environ. Sci. Technol.* **2011**, *45*, 4046.

[23] C. E. Freye, N. A. Crane, T. B. Kirchner, M. J. Sepaniak, *Anal. Chem.* **2013**, *85*, 3991.

[24] C. Wang, F. Cheng, Y. Wang, Z. Gong, M. Fan, J. Hu, *Anal. Methods* **2014**, *6*, 7218.

[25] Z. M. Zhang, J. F. Liu, R. Liu, J. F. Sun, G. H. Wei, *Anal. Chem.* **2014**, *86*, 7286.

[26] Q. Zhu, Y. Cao, D. Li, F. Fang, F. Lu, Y. Yuan, *New J. Chem.* **2019**, *43*, 13873.

[27] A. Tan, Y. Zhao, K. Sivashanmugan, K. Squire, A. X. Wang, *Food Control* **2019**, *103*, 111.

[28] R. A. Wallace, N. V. Lavrik, M. J. Sepaniak, *Electrophoresis* **2017**, *38*, 361.

[29] B. bin Zhang, Y. Shi, H. Chen, Q. xia Zhu, F. Lu, Y. wei Li, *Anal. Chim. Acta* **2018**, *997*, 35.

[30] B. S. Lee, D. Z. Lin, C. H. Huang, T. J. Yen, *J. Raman Spectrosc.* **2018**, *49*, 1920.

[31] B. S. Lee, P. C. Lin, D. Z. Lin, T. J. Yen, *Sci. Rep.* **2018**, *8*, 2.

[32] S. Mennickent, M. De Diego, M. Vega, *Chromatographia* **2013**, *76*, 1233.

[33] W. Wang, T. Gutu, D. K. Gale, J. Jiao, G. L. Rorrer, C. Chang, *J. Am. Chem. Soc.* **2009**, *131*, 4178.

[34] B. Samiey, A. R. Toosi, *J. Hazard. Mater.* **2010**, *184*, 739.

[35] Y. Guo, J. Yu, C. Li, Z. Li, J. Pan, A. Liu, B. Man, T. Wu, X. Xiu, C. Zhang, *Opt. Express* **2018**, *26*, 21784.

[36] J. Xu, C. Li, H. Si, X. Zhao, L. Wang, S. Jiang, D. Wei, J. Yu, X. Xiu, C. Zhang, *Opt. Express* **2018**, *26*, 21546.

[37] J. Yu, Y. Guo, H. Wang, S. Su, C. Zhang, B. Man, F. Lei, *J. Phys. Chem. Lett.* **2019**, *10*, 3676.

[38] C. Zhang, C. Li, J. Yu, S. Jiang, S. Xu, C. Yang, Y. J. Liu, X. Gao, A. Liu, B. Man, *Sens. Actuators, B* **2018**, *258*, 163.

[39] C. Zhang, S. Z. Jiang, Y. Y. Huo, A. H. Liu, S. C. Xu, X. Y. Liu, Z. C. Sun, Y. Y. Xu, Z. Li, B. Y. Man, *Opt. Express* **2015**, *23*, 24811.